Dynamical Simulation of Heavy-Ion Collisions in the Energy Range from a Few Tens MeV/A to a Few Hundreds MeV/A

M.V. Garzelli

Dipartimento di Fisica, Università degli Studi di Milano & INFN, via Celoria, 16
I-20133 Milano, Italia

Abstract. The overlapping stage of heavy-ion reactions can be simulated by dynamical microscopical models, such as those built on the basis of the Molecular Dynamics (MD) approaches, allowing to study the fragment formation process. The present performances of the Quantum MD (QMD) code developed at the University of Milano are discussed, showing results concerning fragment and particle production at bombarding energies up to $\lesssim$ 700 MeV/A, as well as a preliminary analysis on the isoscaling behaviour of isotopic yield ratios for reactions with isospin composition N/Z in the (1–1.2) range, at a 45 MeV/A bombarding energy.

1 Introduction

In the phase diagram of nuclear matter two different regions, where signals related to the probable onset of phase transitions have been detected, have been explored with increasing interest. First of all, a phase-transition is expected to occur at a critical temperature of a few MeV and a critical density relatively low compared to the normal nuclear matter density. Subsaturation densities can be accessed by heavy-ion collisions in the intermediate energy domain (30 MeV/A – 200 MeV/A), which allow to study the thermodynamic properties of strongly interacting nuclear matter. The characteristic features of nuclear forces (long-range attraction and short-range repulsion) could be responsible of the so called liquid-gas phase transition in this region. Symmetry energy effects and Coulomb effects are recognized to play an important role, whereas the role of the nucleon spin has still to be investigated [1]. Reactions in this energy domain are currently studied by means of a number of facilities worldwide. In particular, we mention the experiments performed by the INDRA Collaboration at Ganil, by the ALADIN Collaboration at GSI, and by the CHIMERA and ISOSPIN Collaborations at the LNS in Catania. On the other hand, relativistic and ultrarelativistic energy heavy-ion collisions can be used to explore a region at much higher (ρ, T) where another phase transition probably occurs: the one from hadronic matter made of baryons and mesons to the quark-gluon phase, already investigated at RHIC, and which will be further explored by the LHC heavy-ion program. According to lattice calculations, the critical temperature for the last phase transition or sudden cross-over into a deconfined quark-gluon plasma, is expected

to be ≈ 180 MeV. In this paper we will focus on the first kind of reactions, with projectile energies in the range from tens MeV/A to a few hundreds MeV/A.

Among the possible signatures of a liquid-gas phase transition, we mention in particular multifragmentation, *i.e.* the simultaneous breakup of an excited nuclear system in a large number of IMF (Intermediate Mass Fragments, $3 \leq Z \leq Z_{\rm max}$, where $Z_{\rm max}$ is well below the total charge of the nuclear system) (liquid phase), coexisting in case with LMF (Light Mass Fragments, $Z < 3$) (gas phase). Multifragmentation is a universal phenomenon observed in intermediate-energy nuclear interactions induced by hadrons/photons/heavy-ions [2]. During the overlapping stage of heavy-ion collisions (typical time $\approx$ 100–200 fm/c), depending of the projectile ion bombarding energy and impact parameter, the nuclear system can undergo compression and reach high excitation energies. As a consequence, it starts to expand and can go on expanding down to sub-saturation densities ($\rho \approx 0.1 - 0.3\,\rho_0$, where ρ_0 is the normal nuclear density) and reach temperatures $T \approx 3 - 8$ MeV, where it becomes unstable and breaks up into multiple fragments. These conditions are typical of the liquid-gas mixed phase [3].

One of the issues still open is if a thermal equilibration is reached in these reactions. The statistical description of multifragmentation relies on this assumption. According to this approach, the emissions from multifragmenting sources are not affected by the dynamics which have led to source formation. Only the source global thermodynamical properties are important to determine the fragment pattern. The dynamical description of multifragmentation instead does not rely on this assumption. According to the dynamical approach, multifragmentation is a fast process, and the IMF detected as reaction products are related to nucleon-nucleon correlations already occurring during the ion-ion overlapping stage and surviving the following expansion phase (memory effects) [4].

The fast stage of heavy-ion collisions can be simulated by means of Monte Carlo dynamical models, such as the Quantum Molecular Dynamics ones (QMDs), allowing to describe phase-space fluctuations in the ion-ion overlapping stage, which lead to fragment formation [5]. These are microscopical models, at nucleon level. Preferring a microscopical model to a macroscopical one is mainly motivated by the fact that a large number of degrees of freedom can appear in a reaction. Depending on the bombarding energy of the projectile system and on the impact parameter, one has to consider that excitation and deformation of projectile and target ions, neck formation and breaking, nucleon transfer, different way of fragmenting the composite system, and many other effects can simultaneously play a role [6]. It could be very difficult to take into account so many degrees of freedom in a macroscopical model. In a microscopical dynamical model, on the other hand, they can be described in a more natural, automatic and unified way.

At the end of the fast stage ($\approx 10^{-22}$ s) of ion-ion interactions simulated by QMDs, excited fragments can be present. In order to reproduce experimental data concerning particle and fragment emission, also the de-excitation process has to be accounted for. Fragment de-excitation takes place on a time scale ($\approx 10^{-21}$–10^{-15} s) far larger than the ion-ion overlapping process and is thus more precisely

and faster described by other models. Anyway, some attempts to extend dynamical simulations up to a few thousands fm/c (*i.e.* $\lesssim 10^{-20}$ s) have also been carried out with success by means of modified advanced versions of QMD (see *e.g.* [7]).

In this paper, the QMD code developed in Milano [8, 9] is used to simulate the overlapping stage of ion-ion collisions, leading to excited fragments (prefragments). Primary fragments are identified at the end of each QMD event ($t \approx$ 200–250 fm/c) by applying a phase-space correlation algorithm to the nucleon distribution. Two particles are supposed to belong to the same cluster if their relative distance and momentum are within fixed amounts. Our QMD code has been interfaced to the fragment de-excitation model already implemented into the general purpose FLUKA transport and interaction code [10–12]. The evaporation/fission/Fermi break-up module [13] available in FLUKA allows to describe primary fragment de-excitation on a statistical basis. General features of both codes have been presented in previous papers. In this paper, results of simulation concerning particle and fragment emission at energies within a few hundreds MeV/A are shown and compared to experimental data available in literature. In particular, the code has been applied both to the simulation of heavy-ion collisions up to $\lesssim 700$ MeV/A, as described in Section 2 and 3, and to the study of isospin effects at energies ≈ 50 MeV/A, typical of multifragmentation events, as explained in Section 4. Our conclusions, with some reference to practical applications too, are given in Section 5.

2 Particle Production

As far as thin targets are concerned, double-differential neutron production cross-sections for inclusive reactions at energies around a few hundreds MeV/A have been presented in Ref. [8]. Target thickness has been neglected in our simulations.

As far as thick targets are concerned, a recent paper [14] claimed that old data on neutron double-differential yields, published in previous papers [15,16] by the same working group, suffer from an underestimation of the neutron detector efficiencies, with errors increasing with increasing neutron energy. The authors of [14] have thus re-evaluated the old results taking into account updated estimates of the detection efficiencies and published new data from recent measurements. We simulate the same reactions, taking into account target thicknesses, chosen in the experiment in such a way that the energy losses of projectile ions lead to their stop inside the targets. The results of our theoretical simulations of neutron emission from C and Ne beams impinging on C, Al and Cu systems at a 400 MeV/A bombarding energy are shown in Figure 1 together with both the re-evaluated and the old experimental data, where available. It is apparent that, even if, in general, the results of the theoretical simulations better agree with the re-evaluated data than with the old ones as far as the tails at higher energies are concerned, there are energies/angles where the theoretical simulations better agree with the old data than with the re-evaluated ones. In particular, in case of C projectiles, the results of the simulations always overestimate the experimental data for the emission of high-energy neutrons at a $\sim 60^{\circ}$ angle. The same trend at 60° has been retrieved by using a completely independent

code, *i.e.* the PHITS code [18] including the JQMD model [19], as shown in [14]. These facts point out that, besides the uncertainties indeed present in the models for theoretical simulations, further uncertainties in the experimental data could exist.

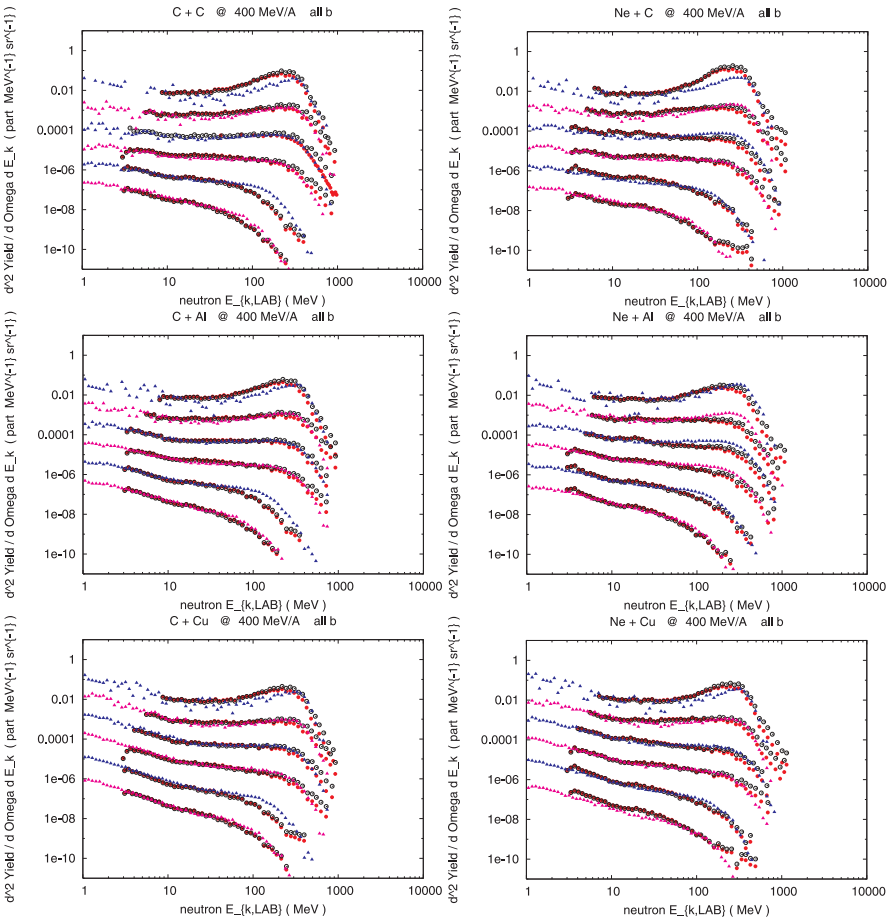

Figure 1. Double-differential neutron production yield for C (left) and Ne (right) projectiles impinging on C (top), Al (center) and Cu (bottom) at a 400 MeV/A bombarding energy. The results of the theoretical simulations made by QMD + FLUKA are shown by solid triangles, whereas the experimental data re-evaluated by Satoh *et al.* [14] are shown by filled circles. The old experimental data [17] are shown by empty circles. In each panel, distributions at 0°, 7.5°, 15°, 30°, 60°, 90° angles with respect to the incoming beam direction in the laboratory frame, have been multiplied by decreasing powers of 10, for display purposes.

3 Fragment Production

As far as fragment production is concerned, we calculate projectile-like fragment production cross-sections for Cl and Ar projectiles impinging on C, Al, Cu and Pb targets at a 650 MeV/A bombarding energy. Experimental data concerning these reactions were taken at the NSRL at the Brookeven National Laboratory, US and at the HIMAC at the National Institute of Radiological Science, Japan and published in Ref. [20]. The results of our simulations are shown together with the experimental data for Ar and Cl projectiles in Figures 2 and 3, respectively. Despite the overall reasonable agreement, it is apparent that the theoretical simulations underestimate the production of the most massive fragments, in case of the most massive targets. These fragments are emitted in very peripheral collisions. A reason of this underestimation can be ascribed to electromagnetic dissociation, which increases with the system mass and was not accounted for by our simulations. Anyway, we estimated that this effect is not enough to explain all discrepancies. On the other hand, for lighter fragments, corresponding to less peripheral collisions, the agreement between theoretical expectations and experimental data is more reasonable and the odd-even effect observed in experimental data is reproduced by the simulation. In our simulations the last feature can be ascribed to de-excitation emission effects. For the lightest fragments which can be identified by the experiment the agreement is sometimes slightly worser. The experimental procedure allows charge identification by means of the ΔE deposited in silicon detectors. With decreasing charge, the

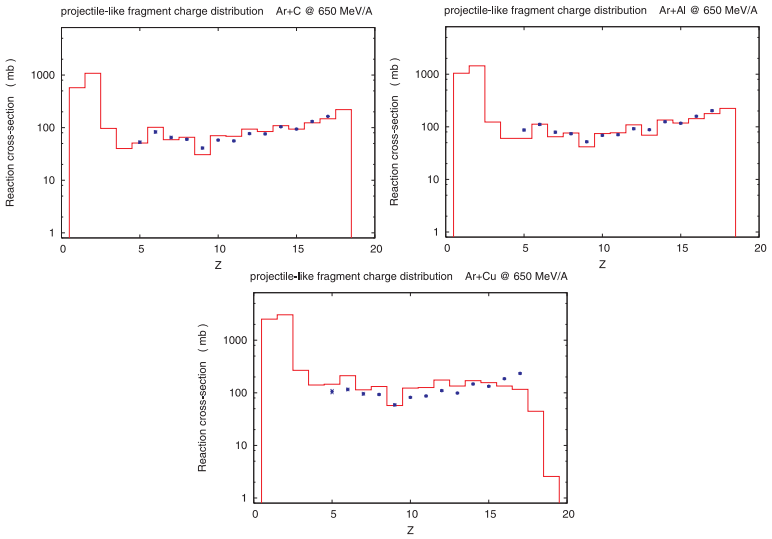

Figure 2. Projectile-like fragment production cross sections for 650 MeV/A Ar beams fragmenting on C (top left), Al (top right) and Ar (bottom) targets, calculated by QMD + FLUKA (solid histograms) in comparison with experimental data taken from Ref. [20] (points). For $Z = 1$ only the contributions to the cross-sections due to fragments ($A > 1$) are shown.

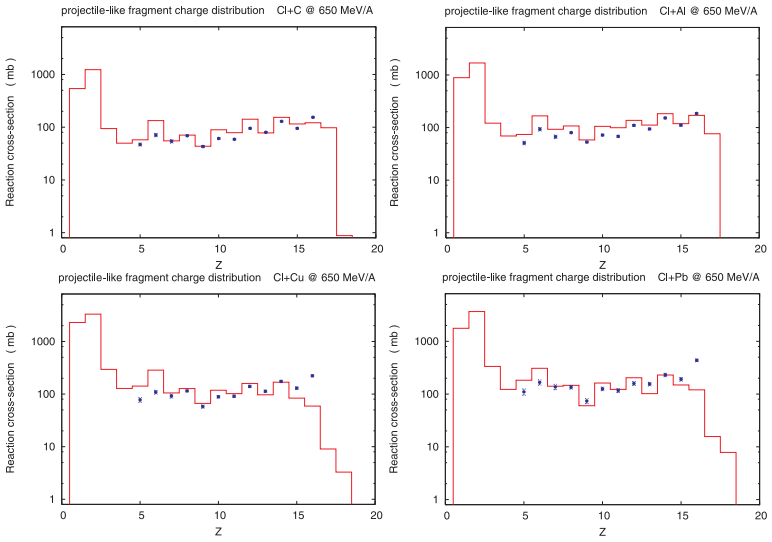

Figure 3. Projectile-like fragment production cross sections for 650 MeV/A Cl beams fragmenting on C (top left), Al (top right), Ar (bottom left) and Pb (bottom right) targets calculated by QMD + FLUKA (solid histograms) in comparison with experimental data taken from Ref. [20] (points). For $Z = 1$ only the contributions to the cross-sections due to fragments ($A > 1$) are shown.

peaks in the (Z, count of events) plots which allow charge identification become increasingly broader [20]. For $Z_{\rm frag} < Z_{\rm primary}/2$ it was not possible to distinguish the peaks corresponding to different charges with the large-acceptance ($\sim 5^{\rm o} - 13^{\rm o}$) detectors used in the experiment. Thus, experimental data were obtained for fragments in the range $5 \leq Z_{\rm frag} < Z_{\rm primary}/2$ by using small acceptance ($\sim 1^{\rm o} - 2^{\rm o}$) detectors. Furthermore, while the detectors measure fragmentation within a small angle around the beam axis, the angular distributions of lighter fragments are less peaked in forward direction. Thus, in our opinion, the uncertainties in charge identification together with those on the estimation of the correction due to the broadness of the angular distributions could largely affect the results on the cross-sections for light fragment production.

The same trend has also been observed in case of different projectiles. The results for Fe + H, Fe + C and Fe + Al at 400 and 500 MeV/A bombarding energies are plotted in the three panels of Figure 4. The agreement between the results of our theoretical simulations and the experimental data [21] is well within 30–35% for most fragments. The QMD + FLUKA interface gives more reliable results in case of heavy targets than in case of the hydrogen one. In case of the H target, the largest discrepancies have been obtained for the lightest fragments (Z = 12 – 16) detected by the experiment (the threshold for charge identification in these experiments was $Z = 12$) at the lowest bombarding energy, whereas a better agreement between theory and experiment is observed for the Z = 22 – 25 fragment production

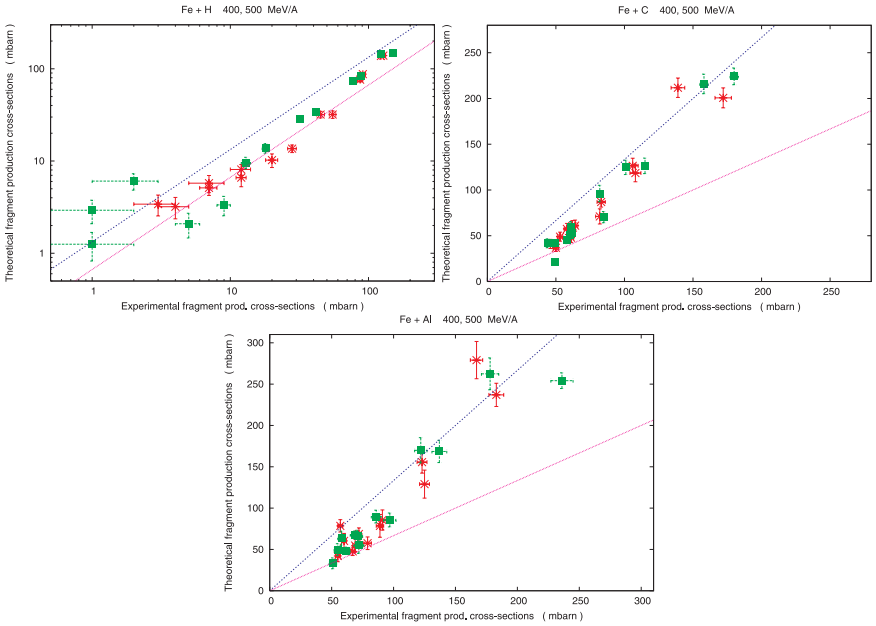

Figure 4. Scatterplots of fragment production cross-sections predicted by QMD + FLUKA de-excitation (vertical axis) vs. experimental cross-sections [21] (horizontal axis) for Fe ions impinging on H (top left), C (top right) and Al (bottom) ions at 400 (crosses) and 500 (squares) MeV/A bombarding energies. The errorbars on the theoretical results are statistical only. The two lines respectively above and below the diagonal correspond to deviations of the modelled results from the experimental ones by $\pm$ 33%.

cross-sections. In case of C and Al targets, the best agreement is observed for the Z = 14 – 21 fragments, whereas the largest discrepancies are seen for the $Z = 24$ fragment cross-section, overpredicted by the theory. The question about the dependence of these results on the target initial configuration need further investigation. Up to now, we use only a few selected projectile and target ion configurations to perform our simulations, giving rise to different events by rotating in a random way the coordinates of these nuclei. The simulations can be carried out as well by choosing a larger number of initial configurations (always satisfying some criteria concerning mean square radius, binding energies, *etc.*) and one can study if this affects the results obtained for the most peripheral collisions. In fact, the most peripheral collisions are expected to be more sensitive than the central ones to properties of the initial ion configurations such as root mean square radius oscillations.

Further effects are still lacking in our and in other QMD models. Among the others, we mention shell effects, a spin-orbit term in the Hamiltonian, ground state deformation of initial nuclei. In particular, accounting for shape deformation can be important for very heavy systems, since fusion/fission reactions are sensitive to the geometry of the collision and the relative orientation of the deformed nuclei. While

the last effects can indeed be included by means of a proper choice of the initial nuclear states, introducing shell effects into a transport model is still a task of great difficulty [6].

Furthermore, a proper treatment of antisymmetrization is still lacking in our model. However, it has already been included in some antisymmetrized advanced versions of QMD like AMD [22] and FMD. These ones are slower, and have mainly been used to study nuclear structure properties, especially for light nuclei, even if several examples of simulation of nuclear reactions with AMD have recently been produced.

4 Isoscaling Observables

The isoscaling technique allows to obtain useful information concerning the symmetry energy of isospin asymmetric nuclear matter, one of the most uncertain and most discussed quantities. This information is important to understand the mechanisms which regulate neutron star formation and structure, collapses of massive stars and supernova explosions. Both in theoretical simulations of nuclear collisions and in experiments the isotopic yield ratio from two reactions with similar total sizes and temperatures, but different isospin asymmetries $(N-Z)/(N+Z)$, has been found to follow an exponential law [23, 24]:

$$\frac{Y_{(2)}(N,Z)}{Y_{(1)}(N,Z)} = \exp(\alpha(Z)N + K(Z)) \tag{1}$$

where the index 2 refers to the reaction with the largest neutron number (more asymmetric) and the index 1 refers to the reaction with the largest proton number (more symmetric). This relation is valid at fixed Z, limiting to the isotopes (N,Z) for which the isotopic yield distributions can be approximated by gaussians. This means that the logarithm of the yield ratio is linear in N, at fixed Z, with a slope given by $\alpha(Z)$. An analogous relation is valid at fixed N, meaning that the yield ratio is also linear in Z. This result is known as the isoscaling phenomenon and has been extensively studied [25, 26]. Among the others, systematic experiments were performed at the Cyclotron Institute of TAMU and at the NSCL of MSU, analyzing the systems Ca + Ni, Ar + Ni, Ar + Fe at 25, 33, 45 and 53 MeV/A bombarding energies [27]. The experimental isotopic yield ratios for light fragments show a linear dependence on N at fixed Z in the logarithmic plane, with $\alpha(Z)$ well approximated by a constant α for each fixed bombarding energy and couple $(1,2)$ of reactions. The results have been interpreted by the authors of [27] both in the framework of the AMD dynamical model and in the framework of a statistical model. We have made simulation of the Ca + Ni, Ar + Fe and Ar + Ni reactions at 45 MeV/A using the QMD model interfaced to the FLUKA de-excitation module. The isospin compositions N/Z for Ca + Ni, Ar + Ni and Ar + Fe amount to $\approx$ 1.04, 1.13 and 1.18, respectively. Our results for the isotopic yield ratios at the end of the whole simulation are plotted in Figure 5. In each panel, also the results for the lightest fragments ($Z = 1$, $Z = 2$)

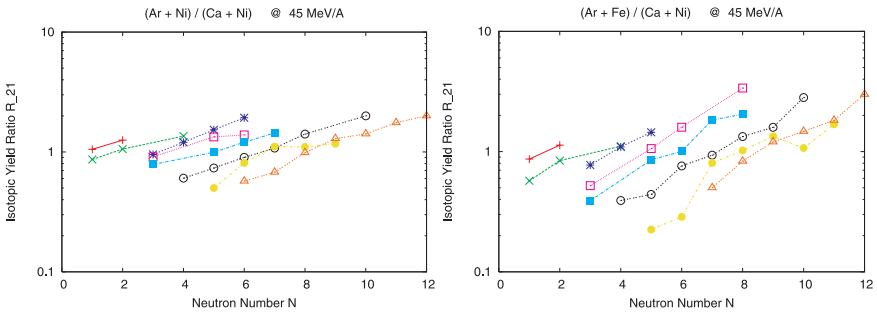

Figure 5. Fragment isotopic yield ratios obtained at the end of our simulations by QMD + FLUKA de-excitation, as a function of N for a 45 MeV/A beam energy. The ratios for the Ar + Ni / Ca + Ni and Ar + Fe / Ca + Ni couple of reactions are shown in the left and in the right panel, respectively. The different symbols correspond to different values of Z in the Z = 1 – 8 (from the left to the right of each panel) range.

are included. It is apparent from our simulation that the linear dependence on N of the fragment yield ratios at fixed Z is a good approximation of the results in the logarithmic plane. Slight deviations from this linear dependence can be due to low statistics ($\approx$ 10000 events distributed over all possible impact parameters were simulated for each reaction). By comparing the left and the right panel it is evident that larger slopes are found for the yield ratios from the couple of reactions with larger difference in the isospin compositions ($N_2/Z_2 - N_1/Z_1$). This behaviour is expected and in qualitative agreement with the experimental observations. However, we observe values of α which differ with Z. We calculate an average α value using the $\alpha(Z)$ values in the Z = 3 – 7 range. We obtain average α values $\approx$ 0.18 and $\approx$ 0.31, for the Ar + Ni / Ca + Ni and Ar + Fe / Ca + Ni ratios, respectively. These values are larger that the ones observed experimentally. A reason of these discrepancies is the fact that only the fragments detected around a $44^{\rm o}$ angle were selected for performing the experimental isoscaling analysis, whereas we consider all fragments, independent of the emission angles. This means that in the experiment the largest contribution to the selected fragments comes probably from central collisions, and these fragments are expected to include nucleons from both the projectile ion and the target one, whereas in our inclusive simulations IMF from projectile-like or target-like residues de-excitation are included. A preliminary analysis on our simulated events show that the α value is indeed affected by the choice of the impact parameter, and decreases significantly when selecting only the most central events. This behaviour is in qualitative agreement with Ref. [23], which claims that isoscaling is observed for a variety of reaction mechanisms, from multifragmentation to evaporation and DIS events, with different slopes in the logarithmic plane. Furthermore, we can observe that the results of our analysis are quite sensitive to the number of isotopes included in the linear fit at fixed Z or, in other words, to the goodness of the gaussian approximation to the fragment isotopic distributions. The last ones are plotted for fragments with Z = 3 – 6 in Figure 6. In each panel the

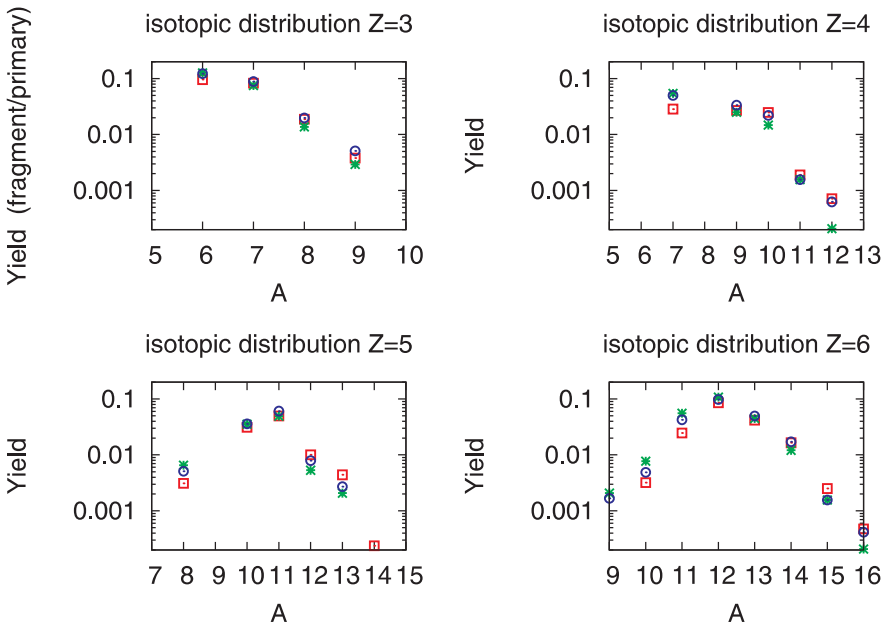

Figure 6. Fragment isotopic distributions for Li, Be, B and C produced by Ca + Ni (stars), Ar + Ni (circles) and Ar + Fe (squares) reactions at a 45 MeV/A bombarding energy, at the end of our simulations by QMD + FLUKA de-excitation.

isotopic distributions from the three considered reactions are plotted together. The isotopic distributions for the emission of light fragments turn out to show memory of the initial isospin content of the system of reacting ions. When comparing the results for the three reactions, it is apparent that the reaction with the smallest asymmetry (or the smallest N/Z value) gives rise to isotopic distributions with larger tails at smaller N, whereas the one with the largest asymmetry (or the largest N/Z value) gives rise to larger tails at larger N. This result is in qualitative agreement with experimental observations. This behaviour is expected to become even more evident at lower bombarding energies.

When considering the free particles emitted in the fast stage of the collision, our QMD simulation suggests that the average yield of emitted protons is larger than the one of emitted neutrons in the Ca + Ni reaction, which has the lowest N/Z value. The other reactions exhibit the opposite trend for the collisions at low impact parameters. This behaviour is due to Coulomb force. In particular, according to our simulations, at pre-equilibrium, the yield of protons Y_p emitted in Ca + Ni central collisions is a fraction $\approx 20\%$ larger than the yield of emitted neutrons Y_n, whereas Y_p is $\approx 10\%$ and 15% smaller than Y_n for Ar + Ni and Ar + Fe central collisions, respectively.

We have also investigated up to which extent the values of α are sensitive to the use of the final fragments (from the full simulation) or the use of the primary

excited fragments in performing the yield ratio analysis. We have found that, for the reactions considered in this study, the average value of α at the end of the overlapping stage of the collisions described by QMD, denoted by α_{hot}, can be larger than the value of α at the end of the full simulation including de-excitation effects by no more than $\approx 20\%$.

Finally, we calculate the fragment asymmetry $(Z/A)^2_{\rm liq}$ of the liquid phase for the three reactions at $t = 250$ fm/c. According to Ref. [23], the liquid phase is defined as composed by all fragments with $A > 4$. For central collisions in each of the three systems the average $(Z/A)^2_{\rm liq}$ at the end of the pre-equilibrium stage turns out to be lower then the corresponding value at $t = 0$, as already found for the same reactions at a lower energy by [27], with a difference between the values at different time more evident for the most symmetric reaction (Ca + Ni). The dependence of the average $(Z/A)^2_{\rm liq}$ on time and impact parameter is under further investigation.

5 Conclusions and Practical Applications

A few examples of the application of the QMD code developed in Milano and interfaced to the FLUKA de-excitation module have been produced, in the simulation of heavy-ion collisions both at a low bombarding energy ($E \approx 50$ MeV/A) and at a few hundreds MeV/A beam energies, showing results which are in agreement, at least from a qualitative point of view, with experimental data and/or previous studies. The studies at low bombarding energies are mainly driven by theoretical issues and are aimed at gaining a better understanding of the role of isospin in multifragmentation processes and in astrophysical mechanisms crucial to determine the evolution of supernovae and neutron stars, and can give insights on the optimization of the production of rare isotopes far from stability. On the other hand, the possibility of extending simulations by the same model even at higher bombarding energies allows to cover application purposes too.

Among the practical application of QMD models we mention hadrontherapy, civil aviation and space radiation protection, and single-event effects in microelectronics. As far as hadrontherapy is concerned, ion beams (in particular C beams) are used to produce Complex Lesions, *i.e.* multiple breaks of the DNA double strands contained in cells. This effect can be exploited in order to kill tumours. This application requires the integration of nuclear models with radiobiological models. In particular, the ion biological effectivenesses turn out to be larger than the X-ray and proton ones. A few facilities built on the basis of these principles already exist (*e.g.* in Japan and in Germany, at GSI and in Heidelberg) or are under construction (*e.g.* the CNAO in Pavia, Italy). At higher energies, crews in space missions and in airflight are exposed to Galactic Cosmic Rays (GCR). Spacecraft and aeroplanes have to be carefully designed in order to minimize GCR interaction effects [28]. Furthermore, functional upset of microelectronic memory devices (silicon chips) in space missions can also occur and deserves particular attention [29]. This phenomen can even take place at sea level, due to atmospheric neutrons (produced in the interactions of Cosmic Rays with air) in the 50–1000 MeV energy range.

Acknowledgments

The author is grateful to D. Satoh for useful discussions and for providing experimental data concerning neutron emission from heavy-ion reactions in thick targets. Collaboration with F. Ballarini, G. Battistoni, F. Cerutti, A. Fassò A. Ferrari, E. Gadioli, A. Ottolenghi, L.S. Pinsky, J. Ranft, P.R. Sala is acknowledged. The FLUKA code is copyrighted by INFN-CERN and is available on the web at `http://www.fluka.org`. This work is supported by the University of Milano.

References

1. S. J. Lee, A. Z. Mekjian, *Phys. Rev. C* **77**, 054612 – 1,15 (2008).
2. J.P. Bondorf, A.S. Botvina, A.S. Iljinov *et al.*, *Phys. Rep.* **257**, 133 (1995).
3. N. Buyukcizmeci, A.S. Botvina, I.N. Mishustin *et al.*, *Phys. Rev. C* **77**, 034608 – 1,7 (2008).
4. K. Zbiri, A. Le Fevre, J. Aichelin *et al.*, *Phys. Rev. C* **75**, 034612 – 1,13 (2007).
5. J. Aichelin, *Phys. Rep.* **202**, 233 – 360 (1991).
6. J. Tian, X. Wu, K. Zhao *et al.*, *Phys. Rev. C* **77**, 064603 – 1,11 (2008).
7. M. Papa, T. Maruyama, A. Bonasera, *Phys. Rev. C* **64**, 024612 – 1,6 (2001); M. Papa, G. Giuliani, A. Bonasera, *J. Comput. Phys.* **208**, 403 (2005).
8. M.V. Garzelli, P.R. Sala, F. Ballarini *et al.*, *Adv. Space Res.* **40**, 1350 – 1356 (2007).
9. M.V. Garzelli, arXiv:0704.3917[nucl-th], Proceedings of ND2007, Int. Conf. on Nuclear Data for Science and Technology, April 22–27 2007, Nice, France, editors O. Bersillon, F. Gunsing, E. Bauge, R. Jacqmin, and S. Leray, EDP Sciences, 1129 – 1132 (2008).
10. A. Ferrari, P.R. Sala, A. Fassò, and J. Ranft, CERN Yellow Report 2005-10, INFN/TC_05/11, SLAC-R-773, 1 – 387 (2005).
11. F. Ballarini, G. Battistoni, M. Brugger *et al.*, *Adv. Space Res.* **40**, 1339 – 1349 (2007).
12. G. Battistoni, S. Muraro, P.R. Sala, F. Cerutti, A. Ferrari, S. Roesler, A. Fassò, J. Ranft, Proceedings of the Hadronic Shower Simulation Workshop 2006, Fermilab 6–8 September 2006, M. Albrow, R. Raja eds., *AIP Conf. Proc.* **896**, 31 – 49 (2007).
13. A. Ferrari, P.R. Sala, Proceedings of the Workshop on Nuclear Reaction Data and Nuclear Reactors Physics, Design and Safety, Trieste, Italy, April 1996, A. Gandini, G. Reffo eds., 2 – 424 (1996).
14. D. Satoh, T. Kurosawa, T. Sato *et al.*, *NIM A* **583**, 507 – 515 (2007).
15. T. Kurosawa, N. Nakao, T. Nakamura *et al.*, *J. Nucl. Sci. Technol.* **36**, 41 (1999).
16. T. Kurosawa, N. Nakao, T. Nakamura *et al.*, *Nucl. Sci. Eng.* **132**, 30 (1999).
17. D. Satoh, private communication.
18. H. Iwase, K. Niita, T. Nakamura, *J. Nucl. Sci. Technol.* **39**, 1142 - 1151 (2002).
19. K. Niita, S. Chiba, T. Maruyama *et al.*, *Phys. Rev. C* **52**, 2620 – 2635 (1995).
20. C. Zeitlin, S.B. Guetersloh, L. Heilbronn *et al.*, *Phys. Rev. C* **77**, 034605 – 1,21 (2008).
21. C. Zeitlin *et al.*, `http://fragserver.lbl.gov`
22. A. Ono, *Phys. Rev. C* **59**, 853 – 864 (1998).
23. M.B. Tsang, W.A. Friedman, C.K. Gelbke *et al.*, *Phys. Rev. Lett.* **86**, 5023 - 5026 (2001).
24. A.R. Raduta, F. Gulminelli, *Phys. Rev. C* **75**, 044605 – 1,11 (2007).
25. A. Ono, P. Danielewicz, W.A. Friedman *et al.*, *Phys. Rev. C* **68**, 051601 – 1,5 (2003).
26. D.V. Shetty, S.J. Jennello, and G.A. Souliotis, *Phys. Rev. C* **75**, 034602 – 1,4 (2007).
27. D.V. Shetty, S.J. Jennello, and G.A. Souliotis, *Phys. Rev. C* **76**, 024606 – 1,15 (2007).
28. F. Ballarini, G. Battistoni, F. Cerutti *et al.*, *Adv. Space Res.* **37**, 1791 – 1797 (2006).
29. H. Jaderstrom, Yu. Marin, Yu. Babain, *et al.*, *Phys. Rev. C* **77**, 044601 – 1,11 (2008).